Roughness Exponent of Domain Interface in CoFe/Pt Multilayer Films

Kang-soo Lee[1], Chang-won Lee[2], Young-jin Cho[2], Sunae Seo[2], Dong-Hyun Kim[3], and Sug-Bong Choe[1]

[1]Center for Subwavelength Optics and School of Physics and Astronomy, Seoul National University, Seoul 151-742, Korea
[2]Samsung Advanced Institute of Technology, Suwon 440-600, Korea
[3]Department of Physics and Institute for Basic Research, Chungbuk National University, Cheongju 361-763, Korea

Critical scaling behavior of magnetic domain interfaces is experimentally investigated in Pt/CoFe/Pt single-layer film (type I) and $(CoFe/Pt)_4$ multilayer film (type II). Even though both samples exhibit domain wall propagation with rare nucleation, the domain interface profile is found to be very contrasting. Typical overhanging interfaces, in contrast to smooth interfaces in type I film, are observed in type II film. Both types of the interface profiles obey power laws. In log–log scaling plot of the roughness with respect to the interface segment length, the slopes, i.e., the scaling exponents, are estimated to be 0.66 ± 0.02 and 0.98 ± 0.03 for type I and II films, respectively. These values of the scaling exponents correspond to two distinct criticality classes of the self-affine and self-similar regimes in random-field Ising model, respectively.

Index Terms—**Domain wall, quenched disorder, roughness exponent, scaling behavior.**

I. Introduction

INTERFACES and surfaces are formed by balancing a huge number of factors. Nevertheless, many scientists have devoted their effort to find a small number of fundamental laws underlying in the interface growth dynamics [1]. For instance, the scaling law has successfully explained the critical behaviors in diverse systems with huge degree of freedom. Magnetic systems have been one of the good test systems for studying these scaling laws, since they have a huge degree of freedom with disorders in the formation of the domain interfaces, i.e., domain walls.

The magnetization reversal occurs by several distinct mechanisms—domain wall motion or nucleation, in ferromagnetic films with perpendicular magnetic anisotropy [2]–[4], [16], [17]. For the case of the domain wall propagation with rare nucleation, the roughness evolution has been analyzed by the random-field Ising model [5], [6]. In the model, the roughness is characterized by the log–log scaling laws with a characteristic exponent. The characteristic scaling exponent has been predicted to be unique within a system irrespective to different material parameters [7]. The domain wall roughness exponent α in 2-D system with 1-D interface is theoretically predicted [8]–[10] and experimentally verified [11] to be $\alpha = 2/3$ in Pt/Co/Pt films. The roughness exponent is then used to explain the scaling behavior in the domain wall creep under a small magnetic field [11]–[14]. However, up to now, the roughness exponent has been examined only for single-layered films and its uniqueness has not been tested yet for multilayered films.

This study is motivated to examine whether the roughness exponent persists the uniqueness in multilayered films. For this study, we investigate the roughness exponent of the magnetic domain walls in CoFe/Pt multilayered films with varying the number of bilayers. The magnetic domains and domain walls are observed by use of a time-resolved magneto–optical Kerr-effect (MOKE) microscope. The roughness exponent is found to be sensitive to the number of bilayers—thicker films exhibit larger exponents. The corresponding criticality classes are discussed within the context of the random-field Ising model.

Manuscript received October 09, 2008. Current version published May 20, 2009. Corresponding author: S.-B. Choe (e-mail: sugbong@snu.ac.kr).
Digital Object Identifier 10.1109/TMAG.2009.2018877

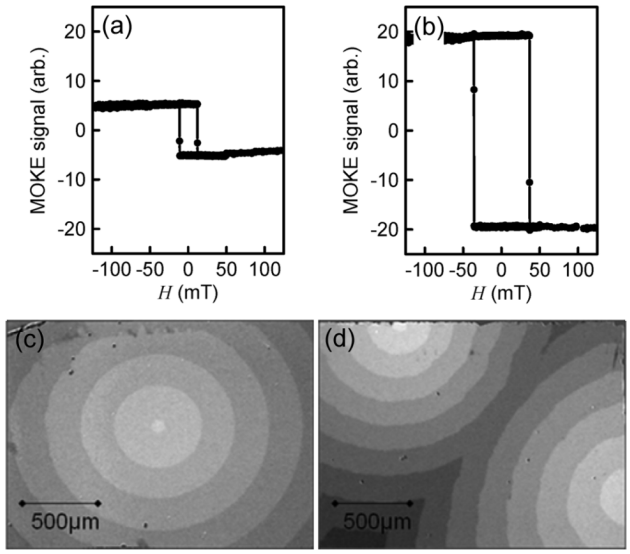

Fig. 1. Polar MOKE hysteresis loops for (a) type I and (b) type II samples, respectively. Typical magnetic domain images captured by a MOKE microscope with a low magnification for (a) type I and (b) type II samples, respectively. The gray contrast corresponds to the domain images taken at different times after applying magnetic field.

II. Experimental Procedure

For this study, 50-Å Ta/25-Å Pt/(5-Å $Co_{90}Fe_{10}$/10-Å Pt)$_n$ multilayered films are deposited on Si substrate with natural SiO_2 layer by direct current (dc)-magnetron sputtering in ultrahigh vacuum environment. Type I samples (5-Å $Co_{90}Fe_{10}$/10-Å Pt)$_1$ and type II samples (5-Å $Co_{90}Fe_{10}$/10-Å Pt)$_4$ are extensively examined. Both films exhibit square hysteresis loops with a strong perpendicular magnetic anisotropy, by means of polar MOKE measurement as shown in Fig. 1(a) and (b). The coercive fields are measured as 11.3 and 36.0 mT for type I and II samples, respectively.

The domain wall configuration is monitored by a time-resolved MOKE microscope, capable of up to $\times 1000$ magnification with an objective lens having the numerical aperture 0.75 with the spatial resolution 0.45 μm. The images are captured

in video rate, and then, analyzed with image processing techniques. The magnetization of the films is first saturated under an external magnetic field sufficiently larger than the coercive field, and then, a small nucleated domain is formed by applying a pulsed magnetic field slightly smaller than the coercive field in the reversed direction. The nucleation takes place reproducibly at a few nucleation sites at which some structural defects are presumably located. By applying pulsed magnetic field repeatedly, the domain wall expands from the nucleated sites. The strength of the magnetic field is chosen to trigger the same domain wall speed for each film, to avoid the possible effect from different domain wall speed. The domain wall speed about 17 ± 2 μm at 23 °C are attained under the strengths of the field, 4.2 and 28.0 mT for type I and II samples, respectively.

Fig. 1(c) and (d) shows the circular expansion of the domain wall from a nucleation site. The images are taken by a MOKE microscope with a low magnification ($\times 25$), to see the overall domain patterns. The gray contrast corresponds to the different domain images taken after applying successive magnetic field pulses. Both samples show clear circular domain wall expansion, which evidences that the magnetization reversal is dominated by the domain wall motion from rare nucleation site. After sufficient propagation for saturation of the growth of the domain wall roughness, the domain wall images are captured with a high magnification ($\times 1000$). The captured domain wall images are then subtracted by the precaptured background image and converted into black and white images. All the image analyses are carried out under the same prescribed condition. Finally, the domain wall profile as an array of the domain wall position is obtained for the roughness scaling analysis.

III. Results and Discussion

Fig. 2 shows the typical domain images of type I [Fig. 2(a)] and type II [Fig. 2(b)] samples, respectively. The images are taken after a sufficient propagation from the nucleation sites to form almost linear profile of the overall domain wall configuration inside the field of view. The figures clearly show that thicker film exhibits rougher domain wall profile. It is worthwhile to note that in addition to the difference in the degree of the roughness, overhanging profiles are observed only in type II sample, whereas smooth profiles are observed in type I sample.

To see the effect on the scaling behavior due to the overhanging profiles, a standard scaling analysis is adopted. From the analysis, one can determine the roughness and the roughness exponent, separately. It is crucial to note that there exists clear distinction between the roughness and the roughness exponent. Even though the roughness is apparently and intuitively seen from the domain wall profiles, the magnetization dynamics is governed mainly by the roughness exponent [11]. The roughness exponent α is related to how the roughness increases with increasing the domain wall segment length L. The roughness exponent is defined as

$$w(L) \propto L^{\alpha} \tag{1}$$

where $w(L)$ is the characteristic roughness with respect to L. It is originally given by [1]

$$w(L) = \left\langle h(x)^2 \right\rangle_L - \langle h(x) \rangle_L^2 \tag{2}$$

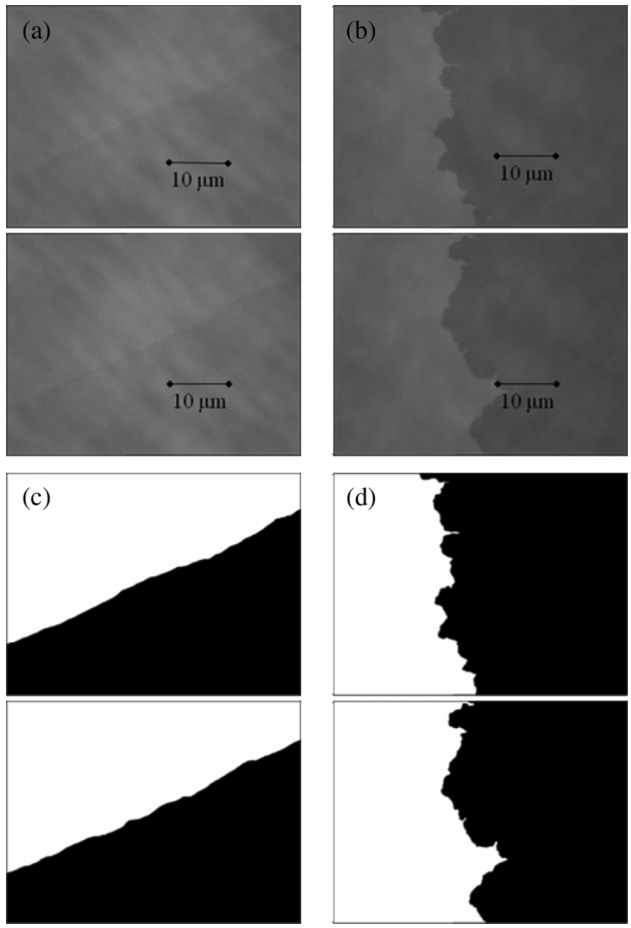

Fig. 2. Typical domain images captured by a MOKE microscope with a high magnification for (a) type I and (b) type II samples, respectively. Two images for each sample are captured on the same area at different runs. The black-and-white images converted after background subtraction are shown in (c) and (d).

where $\langle\ \rangle_L$ designates the average inside all the possible length L. For our system with the whole length S of the images under examination, it is given by

$$w(L) = \frac{1}{S-L} \times \int_0^{S-L} \sqrt{\frac{1}{L}\int_s^{s+L} h^2(x)dx - \left[\frac{1}{L}\int_s^{s+L} h(x)dx\right]^2}\, ds. \tag{3}$$

Here, $h(x)$ is the height grown from the initial domain wall position presumed to be on a straight line. However, since the domain walls are circularly expanded from a single nucleation site in our experimental condition, it is not clear to define the initial line of the domain wall. Therefore, in this study, we introduce a quasi-initial line of the domain wall as the line connecting between the two positions separated by the length L along the domain wall. The height h is then given by the distance normal to the line, and therefore, the roughness is calculated as the standard deviation of the height h. This approach successfully removes the ambiguity of the overall angle of the images. It thus provides a self-consistent and scale-free way to analyze the roughness profiles, irrespective to the initial position of the domain wall. The validity of this approach is limited for small L, since the circular domain wall profile recovers for large L comparable to the radius of the circle. We thus expand

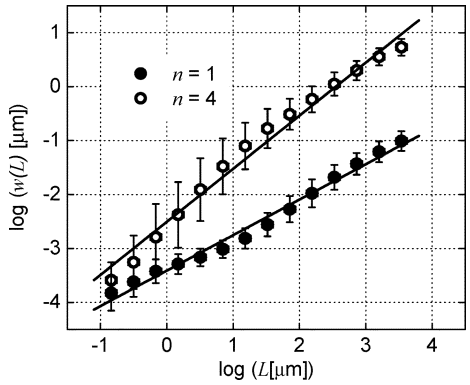

Fig. 3. The log–log scaling plot of the roughness w with respective to the domain wall segment length L. The solid and open symbols correspond to type I and type II samples, respectively.

the circular domains with the radius larger than 3 mm, and then, analyze a small area of $L < 100$ μm, which corresponds to the 2° arc of the overall circular domains.

Fig. 3 exhibits the log–log scaling plots for type I (solid symbol) and type II (open symbol) samples. Here, the ordinate is $\log(w)$ and the abscissa is $\log(L)$. It is clearly seen from the figure that the roughness exponent, i.e., the slope of the data, is sensitive to the film thickness—thicker film has larger exponent. Type I sample has $\alpha = 0.66 \pm 0.02$ in accordance with the previous results for single-layered films [11], [13]. On the other hand, type II sample has another distinct value $\alpha = 0.98 \pm 0.03$.

The former value of the scaling exponent is in good agreement with the theoretically predicted value 2/3 for the self-affine regime of the random-field Ising model, whereas the latter value is accordant with the values predicted for the self-similar regime [15]. It is also consistent with the experimental observations that the overhanging profiles are theoretically predicted in the self-similar regime in contrast to smooth profiles without overhanging in the self-affine regime. Thus, one can conclude that there exists a crossover between two different criticality regimes with increasing the number of bilayers—type I sample exhibits the criticality class of the self-affine regime and type II sample exhibits the criticality class of the self-similar regime.

Both self-affine and self-similar regimes are predicted in the random-field Ising model for different characteristic strength Δ of the disorder, respectively [1]. In the model, the quenched disorders are uniformly distributed over the interval $[-\Delta, \Delta]$. The self-affine regime appears for a relatively smaller disorder $2.4 < \Delta < 3.4$, whereas the self-similar regime is for large disorder $\Delta > 3.4$ [1]. In consequence, the roughness profile in the self-affine regime is determined by the counterbalance between the weak structural disorder and the thermal fluctuation. The thermal fluctuation triggers the thermally activated depinning from weak structural disorders to form smooth interface profiles. In contrary, in the self-similar regime, the roughness profile is governed solely by the strong structural disorder. The overhanging profile thus appears by pinning at strong structural disorders sufficiently larger than the thermal fluctuation. It is therefore reasonable to expect that the criticality transition between type I and type II samples is ascribed to the degree of the structural irregularities. It is natural to imagine that thicker film has larger Δ, since the local structural disorders such as atomic misfits, defects, dislocations, and crystalline misorientations are accumulative during the film deposition. The structural disorders cause magnetic irregularities for nucleation and/or domain wall pinning sites [3]. Other possible reasons for these distinct scaling behaviors could be the strength difference of domain wall tension, dipolar interaction, and interlayer coupling strength.

IV. Conclusion

The roughness of the magnetic domain walls is experimentally investigated in ferromagnetic CoFe/Pt multilayered films with perpendicular magnetic anisotropy. The roughness and the roughness exponent are increased with increasing the number of bilayers of the films. We demonstrate a transition between two different critical scaling regimes—self-affine regime and self-similar regime of the random-field Ising model.

Acknowledgment

This study was supported by the KOSEF under the NRL program (R0A-2007-000-20032-0).

References

[1] A. Barabási and H. E. Stanley, *Fractal Concepts in Surface Growth*. Cambridge, U.K.: Cambridge Univ. Press, 1995.

[2] J. Pommier, P. Meyer, G. Pénissard, and J. Ferré, "Magnetization reversal in ultrathin ferromagnetic films with perpendicular anisotropy: Domain observations," *Phys. Rev. Lett.*, vol. 65, no. 16, pp. 2054–2057, Oct. 1990.

[3] S. B. Choe and S. C. Shin, "Phase diagram of three contrasting magnetization reversal phases in uniaxial ferromagnetic thin films," *Appl. Phys. Lett.*, vol. 80, no. 10, pp. 1791–1793, Mar. 2002.

[4] S. B. Choe and S. C. Shin, "Magnetic field dependence of spin reversal behavior in CoPd nanomultilayers," *J. Appl. Phys.*, vol. 87, no. 9, pp. 5076–5078, May 2000.

[5] M. Huth, P. Haibach, and H. Adrian, "Scaling properties of magnetic domain walls in Pt/Co/Pt trilayers on MgO(111)," *J. Magn. Magn. Mater.*, vol. 240, pp. 311–313, 2002.

[6] M. Jost and K. D. Usadel, "Interface roughening in driven magnetic systems with quenched disorder," *Phys. Rev. B, Condens. Matter*, vol. 54, no. 13, pp. 9314–9321, Oct. 1996.

[7] K. S. Ryu, H. Akinaga, and S. C. Shin, "Tunable scaling behaviour observed in Barkhausen criticality of a ferromagnetic film," *Nature Phys.*, vol. 3, pp. 547–550, Aug. 2007.

[8] D. A. Huse, C. L. Henley, and D. S. Fisher, "Respond," *Phys. Rev. Lett.*, vol. 55, no. 26, p. 2924, Dec. 1985.

[9] M. Kardar and D. R. Nelson, "Commensurate-incommensurate transitions with quenched random impurities," *Phys. Rev. Lett.*, vol. 55, no. 11, pp. 1157–1160, Sep. 1985.

[10] M. Kardar, "Replica Bethe Ansatz studies of two-dimensional interfaces with quenched random impurities," *Nucl. Phys.*, vol. B290, pp. 582–602, 1987.

[11] S. Lemerle, J. Ferré, C. Chappert, V. Mathet, T. Giamarchi, and P. Le Doussal, "Domain wall creep in an ising ultrathin magnetic film," *Phys. Rev. Lett.*, vol. 80, no. 4, pp. 849–852, Jan. 1998.

[12] P. Chauve, T. Giamarchi, and P. Le Doussal, "Creep and depinning in disordered media," *Phys. Rev. B, Condens. Matter*, vol. 62, no. 10, pp. 6241–6267, Sep. 2000.

[13] F. Cayssol, D. Ravelosona, C. Chappert, J. Ferré, and J. P. Jamet, "Domain wall creep in magnetic wires," *Phys. Rev. Lett.*, vol. 92, no. 10, p. 107202, Mar. 2004.

[14] C. S. Nolle, B. Koiller, N. Martys, and M. O. Robbins, "Effect of quenched disorder on moving interfaces in two dimensions," *Physica A*, vol. 205, pp. 342–354, 1994.

[15] H. Leschhorn, "Interface depinning in a disordered medium—Numerical results," *Physica A*, vol. 195, pp. 324–335, 1993.

[16] G. P. Zhao, M. G. Zhao, H. S. Lim, Y. P. Feng, and C. K. Ong, "From nucleation to coercivity," *Appl. Phys. Lett.*, vol. 87, p. 162513, Oct. 2005.

[17] G. P. Zhao and X. L. Wang, "Nucleation, pinning, and coercivity in magnetic nanosystems: An analytical micromagnetic approach," *Phys. Rev. B, Condens. Matter*, vol. 74, no. 1, p. 012409, Jul. 2006.